Coulomb blockade of chiral Majorana and complex fermions far from equilibrium

Dmitriy S. Shapiro,[1,2,*] Alexander D. Mirlin,[1,3] and Alexander Shnirman[1,3]

[1]*Institute for Quantum Materials and Technologies (IQMT), Karlsruhe Institute of Technology, 76021 Karlsruhe, Germany*

[2]*Laboratory of Superconducting Metamaterials, National University of Science and Technology MISiS, 119049 Moscow, Russia*

[3]*Institut für Theorie der Kondensierten Materie, Karlsruhe Institute of Technology, 76128 Karlsruhe, Germany*

(Received 12 January 2023; accepted 22 February 2023; published 6 March 2023)

We study charge transport in a single-electron transistor implemented as an interferometer such that the Coulomb-blockaded middle island contains a circular chiral Majorana or Dirac edge mode. We concentrate on the regime of small conductance and provide an asymptotic solution in the limit of high transport voltage exceeding the charging energy. The solution is achieved using an instantonlike technique. The distinctions between Majorana and Dirac cases appear when the tunnel junctions are unequal. The main difference is in the offset current at high voltages which can be higher, up to 50% in the Majorana case. It is caused by an additional particle-hole symmetry of the distribution function of Majorana fermions. There is also an eye-catching distinction between the oscillation patterns of the current as a function of the gate charge. We conjecture this distinction survives at lower transport voltages as well.

DOI: 10.1103/PhysRevB.107.125404

I. INTRODUCTION

The effect of the Coulomb blockade in a single-electron transistor (SET) [1–7], a device where Fermi-liquid leads are mediated by a quantum dot, plays an essential role in condensed matter physics, mesoscopics, and open quantum systems. The Coulomb spectroscopy and transport through a quantum dot are sensitive to the precise nature of the nonequilibrium steady state, the mechanisms of relaxation, electronic interactions, and topological order [8–20]. The "orthodox" theory of the Coulomb blockade is based on rate equations formulated in the basis of different charged states in the island [1–3,5]. Such states are well defined for almost isolated quantum dots which have weak tunnel coupling to the leads, i.e., with a small dimensionless conductance, $g \ll 1$. In this theory, the distribution function in the island is not affected by the the coupling to contacts; i.e., the internal relaxation in the island is assumed to prevail on the characteristic tunneling time scale. In the multichannel limit with $g \gg 1$, when the Coulomb blockade is weak and the charge is ill defined, the description via the dissipative Ambegaokar-Eckern-Schön (AES) action [21,22] for the phase becomes more convenient [8]. In equilibrium, the saddle points of the Matsubara AES action are known as Korshunov instantons [23]. These instantons allow one to take into account charge discreteness and obtain the residual, exponentially small gate charge oscillations of the conductance. If the relaxation is weak then the distribution function in the island is a non-Fermi one at finite voltages. It causes a nonequilibrium steady state that cannot be captured by the "orthodox" theory or the imaginary-time technique, and consequently the real-time Keldysh formalism [24,25] is required. Important recent achievements include the theoretical analysis of strongly nonequilibrium transport using the AES action [10], and the generalization of Korshunov instantons to the real-time Keldysh formalism [15] at $g \gg 1$. In particular, the results of Ref. [10] lead directly to the conclusion that the Coulomb blockade is lifted at transport voltages lower than in the "orthodox" theory due to the nonequilibrium distribution function in the island.

In this work, we study the strongly nonequilibrium regime of high voltages that exceed significantly the charging energy of an island, and we assume a strong Coulomb blockade; i.e., the dimensionless conductance is small, $g \ll 1$. At low voltages one thus expects a strong suppression of the charge transport. At higher voltages the almost Ohmic behavior is accompanied by the offset (deficit) current and residual gate charge oscillations. Here, we were able to describe this high-voltage regime asymptotically exactly. Instead of using the kinetic equations, which is challenging due to a large number of relevant charge states, we employ a path-integral technique and succeed solving the problem by finding a dominant path, an alternative kind of instanton, for the phase variable.

We apply our solution for calculations of the nonequilibrium tunneling density of states (TDoS) and current-voltage relations using the formalism developed by Meir and Wingreen [26]. The devices under consideration are chiral interferometers implemented in hybrid structures with superconductors, topological insulators, or quantum anomalous Hall insulators (QAHIs) [27–29] (see Fig. 1). They have two Fermi-liquid leads biased by the voltages $\pm V/2$, and tunnel coupled to the central island. The island hosts a single conducting channel which is either a real Majorana fermion edge mode (the case when the island is in a proximity-induced topological superconducting phase) or a complex Dirac one (the case of a normal island in a quantum Hall topological insulator state). There is an electrostatic gate that induces an offset charge in the island, Q_g. The charging energy of the

*dmitrii.shapiro@kit.edu

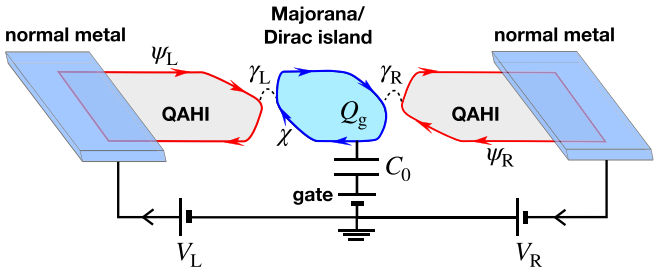

FIG. 1. Sketch of a single-electron transistor realized as chiral Majorana or Dirac interferometer. Normal metal leads (Ohmic contacts) cover spinless channels with chiral Dirac fermions, $\psi_{L,R}$, which are the edges of a quantum anomalous Hall insulator (QAHI) film. Gate voltage controls the offset charge Q_g in the island of capacitance C_0. The island is in the topological superconducting or normal state. The chiral mode χ hosts Majorana or Dirac fermions. Tunnel amplitudes are $\gamma_{L,R}$, and bias voltages are symmetric, $V_{L(R)}=\pm V/2$; the positive direction of the current is marked by black arrows.

island is $E_c = e^2/(2C_0)$ with e the electron charge and C_0 the total capacitance of the island. The chiral fermions propagate with a velocity v along the edge channels. In this case, the Thouless energy, $E_{Th} = \frac{2\pi\hbar v}{L}$ ($\hbar$ is Planck's constant), is nothing but level spacing in the ring of the perimeter L. (Hereafter we set $e = \hbar = 1$.) We assume a metallic spectrum of the edge modes which means that E_{Th} is sufficiently small. The voltages are limited from above by the energy scale Δ_0—the absolute value of the superconducting order parameter induced in the topological part of the island—above which other conducting channels or two-dimensional (2D) scattering states become relevant. Ultimately, we work under the following assumption:

$$\Delta_0 > eV \gg \{E_{Th}, E_c\}. \tag{1}$$

Moreover, we assume no relaxation to phonons, no electron-electron scattering, and zero temperature. The only relaxation mechanism is due to the tunneling to the leads. In this regime the single-particle distribution function is expected to develop a multistep structure which will play a substantial role below.

II. MODEL

A. Keldysh action for the Majorana device

The microscopic description of the charge transport is provided by the Keldysh generating functional

$$\mathcal{Z}[\eta] = \int D[\Psi]D[\chi]D[\varphi]e^{iS[\Psi,\chi,\varphi,\eta]}. \tag{2}$$

The first path integral is taken over complex fermions, $\Psi = \{\Psi_L, \Psi_R\}$, collected in Nambu spinors $\Psi_L = \{\psi_{L,k}, \bar{\psi}_{R,-k}\}$ and $\Psi_R = \{\psi_{R,k}, \bar{\psi}_{R,-k}\}$ where $\psi_{L,k}$ ($\psi_{R,k}$) are Grassmann fields in left (right) leads; these are chiral states of momenta $k \in [-\infty, \infty]$. The second variable $\chi(x)$ is a Majorana edge mode in the island being a real Grassmann field defined on a ring with a coordinate $x \in [0, L]$. The third one, φ, is the phase of the superconducting order parameter in the island. $\mathcal{Z}$ depends on a pair of counting fields η_L and η_R (source variables) collected in $\eta = \{\eta_L, \eta_R\}$. They generate the charges Q_l that flow from the left ($l = L$) or right ($l = R$) lead into the island during the measurement interval $t \in [0; t_0]$:

$$Q_l = i\frac{\partial \mathcal{Z}[\eta]}{\partial \eta_l}\bigg|_{\eta\to 0}. \tag{3}$$

The total action is

$$S = S_c + S_L + S_R + S_M + S_L^{(tun)} + S_R^{(tun)}. \tag{4}$$

In the Keldysh technique, the physical time $t \in [-\infty, \infty]$ gets doubled, $t_\pm$, with the index $\pm$ denoting the upward and backward parts of Keldysh contour $\mathcal{C}$. Then, the Keldysh rotation to classical and quantum components of the boson field, φ_{cl} and φ_q, is performed: $\varphi(t_\pm) = \varphi_{cl}(t) \pm \varphi_q(t)/2$.

A coherent dynamics of φ is governed by the action $S_c = \int \mathcal{L}_c[\varphi]dt$ where the Lagrangian is

$$\mathcal{L}_c = \frac{\dot{\varphi}_q\dot{\varphi}_{cl}}{8E_c} - \frac{1}{2}\dot{\varphi}_q Q_g. \tag{5}$$

Complex fermion dynamics is described by Keldysh actions, $S_l = \int_{\mathcal{C}} dt(\int \frac{dk}{2\pi}\bar{\psi}_{l,k}i\partial_t\psi_{l,k} - H_l)$, where $H_l = \hbar v \int \frac{dk}{2\pi}k\bar{\psi}_{l,k}\psi_{l,k}$ is a Hamiltonian of chiral fermions and the lead index is $l = L, R$. The action in $\pm$ basis reads $S_l = \sum_{\sigma,\sigma'}\iint \frac{d\omega dk}{(2\pi)^2}\bar{\psi}_{l,\sigma}[G^{-1}_{l,\omega,k}]_{\sigma,\sigma'}\psi_{l,\sigma'}$ where the inverted fermion Green function is

$$G^{-1}_{L(R),\omega,k} = (\omega - vk)\sigma^z + i\varepsilon((\sigma^0 + \sigma^x)f_{L(R),\omega} - i\sigma^y), \tag{6}$$

σ^α are the Pauli matrices, and $\varepsilon > 0$ is an infinitesimal broadening constant. We keep the $\pm$ basis for fermions while performing the Keldysh rotation to the classical and quantum components for the phase, φ. The functions $f_l = 1 - 2n_l$ are determined by zero-temperature Fermi distribution functions in the leads, $n_{L(R),\omega} = \frac{1}{2} - \frac{1}{2}\mathrm{sgn}(\hbar\omega \mp eV/2)$. We assume here that the symmetric voltage bias $V_{L(R)} = \pm V/2$ is applied. The energies $\hbar\omega$ of Dirac electrons in the leads are counted from a chemical potential at zero bias.

We apply a uniform gauge transformation (see Appendix A) for the complex fermions $c(\mathbf{r}, t)$ in the island, $c(\mathbf{r}, t) \to e^{-i\mu t - i\frac{1}{2}\varphi(t)}c(\mathbf{r}, t)$. After the transformation, the floating phase $\varphi(t)$ and the yet unknown chemical potential of the s-wave superconducting island, μ, are eliminated from the island's action; they appear instead in the tunneling action below. One arrives at the stationary Bogoliubov–de Gennes Hamiltonian, which at low energies [below Δ_0; see Eq. (1)] reduces to the following effective action for chiral edge Majorana modes:

$$S_M = \frac{1}{2}\sum_{\sigma,\sigma'}\int_0^L dx \int dt\, \chi_\sigma(i\partial_t + iv\partial_x)\sigma^z_{\sigma,\sigma'}\chi_{\sigma'}. \tag{7}$$

Here, the Lagrangian is diagonal in the Keldysh space; i.e., there is no internal broadening or dissipation. In this case, this kernel is not invertible which means fully unitary dynamics. An introduction of an infinitesimal broadening with some distribution functions is not necessary as it will anyway be overridden by the coupling to the leads. The latter is described by the tunnel action for the low-energy modes, where the above-mentioned gauge transformation and the rotation to the

Majorana basis is performed,

$$S_l^{(\mathrm{tun})}[\varphi,\eta]=\gamma_l\sum_{\sigma,\sigma'}\int dt\,\chi_{l,\sigma}(x_l)\big(U[\varphi,\eta_l]_{\sigma,\sigma'}\psi^{(0)}_{l,\sigma'} - U^{+}[\varphi,\eta_l]_{\sigma,\sigma'}\bar{\psi}^{(0)}_{l,\sigma'}\big). \tag{8}$$

Here, the Majorana field $\chi(x)$ couples to the local fermions in the leads $\psi_l^{(0)}=\int\frac{dk}{2\pi}\psi_{l,k}$ at two points, $x=x_{\mathrm{L,R}}$. The tunnel amplitudes γ_l are chosen real. The matrix

$$U[\varphi,\eta_l]=e^{-i\mu t-i\frac{1}{2}\varphi_{\mathrm{cl}}(t)}e^{-i\frac{\varphi_{\mathrm{q}}(t)+2\eta_l z(t)}{4}\sigma^z} \tag{9}$$

captures the gauge transformation mentioned above and the counting field.The yet unknown chemical potential of the island, μ, will be found after solving an appropriate kinetic equation. This transformation also means that all energies in the island are counted from μ. The charge counting variable η_l is an amplitude of the auxiliary quantum field, $\frac{\eta_l z(t)}{2}\sigma^z$. It generates the transmitted charge $Q_l[\varphi]$ which is a classical observable. Further, $z(t)=1$ for $t\in[0,t_0]$ and $z(t)=0$ otherwise. It switches the charge counting on and off at $t=0$ and $t=t_0$, respectively.

B. Nonequilibrium effective theory for the phase

After the integration over the complex fermions, Ψ, and then over the Majorana ones, χ, the generating functional (2) becomes

$$\mathcal{Z}[\eta]=\int D[\varphi]e^{iS_{\mathrm{c}}[\varphi]+\frac{1}{2}\mathrm{tr}\ln((i\partial_t+iv\partial_x)\sigma^z-\Sigma[\varphi,\eta])}. \tag{10}$$

Here, Σ is the self-energy for Majorana fermions. It reads

$$\Sigma[\varphi,\eta]_{x,t,t'}=\sum_{l=\mathrm{L,R}}\gamma_l^2(\mathcal{G}'_l[\varphi]_{t,t'}-[\mathcal{G}'_l[\varphi]_{t',t}]^T)\delta(x-x_l), \tag{11}$$

where $\mathcal{G}'_l[\varphi]_{t,t'}=U_l^+(t)\sigma^z\mathcal{G}_l(t-t')\sigma^zU_l(t')$ is the boson-dressed Green function of the lead. The self-energy Σ is singular at the points where the tunnel contacts are located. The presence of two contributions to the self-energy ($\mathcal{G}'$ and $[\mathcal{G}']^T$) reflects the Majorana nature of the island excitations. In the time domain the local Green functions of the leads read $\mathcal{G}_l(t)=\int\frac{d\omega}{2\pi}\mathcal{G}_{l;\omega}e^{-i\omega t}$, where

$$\mathcal{G}_{l;\omega}\equiv\int\frac{dk}{2\pi}G_{l;\omega,k}=\frac{i}{4\pi v}((\sigma^x-\sigma^0)f_{l;\omega}-i\sigma^y). \tag{12}$$

To analyze the phase dynamics, we develop here an expansion scheme for the logarithm in Eq. (10). A naive expansion in the small tunneling amplitude γ_l would force us to introduce an infinitesimal broadening in the island with an arbitrary distribution function. However, in such an approach a physical distribution function, dictated by the leads, would emerge only after the infinite summation of higher-order contributions. Instead, we extract from $\Sigma[\varphi,\eta]$ a part with a constant-in-time classical phase φ_0, $\Sigma[\varphi,\eta]=\Sigma[\varphi_0,0]+(\Sigma[\varphi,\eta]-\Sigma[\varphi_0,0])$. We transfer the extracted part, $\Sigma[\varphi_0,0]$, into the zero-order propagator [16],

$$\mathbf{G}_0^{-1}=(i\partial_t+iv\partial_x)\sigma^z-\Sigma[\varphi_0,0], \tag{13}$$

which we can invert exactly, and perform an expansion in $\delta\Sigma[\varphi,\eta]=\Sigma[\varphi,\eta]-\Sigma[\varphi_0,0]$. Due to the gauge invariance of the problem, φ_0 does not appear in the final results.

We expand the logarithm in Eq. (10) up to the first order in $\delta\Sigma$. After that, $\delta\Sigma$ itself is expanded up to the linear order in η since we are interested in the current only. Omitting a constant term, we obtain the following result for the logarithm in Eq. (10):

$$\tfrac{1}{2}\mathrm{tr}\ln((i\partial_t+iv\partial_x)\sigma^z-\Sigma[\varphi,\eta]) \approx iS_{\mathrm{AES}}[\varphi]-i\eta_{\mathrm{L}}Q_{\mathrm{L}}[\varphi]-i\eta_{\mathrm{R}}Q_{\mathrm{R}}[\varphi]. \tag{14}$$

The first term in Eq. (14) is the dissipative AES action [21,22],

$$S_{\mathrm{AES}}[\varphi]=i\tfrac{1}{2}\mathrm{tr}[\mathbf{G}_0\delta\Sigma[\varphi,\eta=0]], \tag{15}$$

and the second and third terms contain the charges $Q_l[\varphi]$ [cf. Eq. (3)] calculated for a certain path, $\varphi_{\mathrm{c}}(t)$ and $\varphi_{\mathrm{q}}(t)$. These are given by

$$Q_l[\varphi]=\frac{i}{2}\lim_{\eta\to0}\partial_{\eta_l}\mathrm{tr}[\mathbf{G}_0\delta\Sigma[\varphi,\eta]]. \tag{16}$$

We will denote the frequencies related to the island by ϵ keeping ω for the leads. This helps us to remember that the energies on the island are counted from the chemical potential. Since Σ is singular in coordinate representation [cf. Eq. (11)], one needs to know the Green function $\mathbf{G}_{0,\epsilon}$ at coincident coordinates, $x\to x_l$ and $x'\to x_l$. Comparing the tunneling self-energy and the ballistic propagator, we conclude that the weak-tunneling limit corresponds to the condition $\gamma_l\ll v$. This limit is fully equivalent to the condition of small broadening of levels compared to the distance between them, $\frac{\sqrt{\gamma_{\mathrm{L}}^2+\gamma_{\mathrm{R}}^2}}{L}\ll E_{\mathrm{Th}}$. In this regime, the Green function reads (see Appendix B)

$$\mathbf{G}_{0,\epsilon}=-i\frac{E_{\mathrm{Th}}}{2v}\sum_n\delta(\epsilon-\epsilon_n)((\sigma^0-\sigma^x)f_{\mathrm{M},\epsilon_n}+i\sigma^y), \tag{17}$$

which involves the four-step function

$$f_{\mathrm{M},\epsilon}=\frac{\gamma_{\mathrm{L}}^2(f_{\mathrm{L},\mu+\epsilon}-f_{\mathrm{L},\mu-\epsilon})+\gamma_{\mathrm{R}}^2(f_{\mathrm{R},\mu+\epsilon}-f_{\mathrm{R},\mu-\epsilon})}{2(\gamma_{\mathrm{L}}^2+\gamma_{\mathrm{R}}^2)} \tag{18}$$

describing the non-Fermi distribution of Majorana fermions. It has the symmetry, $f_{\mathrm{M},\epsilon}=-f_{\mathrm{M},-\epsilon}$, which is preserved for arbitrary γ_{L} and γ_{R}.

The function $\mathbf{G}_{0,\epsilon}$ is singular at $\epsilon=\epsilon_n$ where $\epsilon_n=(n+n_v/2)E_{\mathrm{Th}}$ are the energy levels of the island ($n\in\mathbb{Z}$ and n_v is the number of vortices). To calculate the chemical potential we neglect the fluctuations of phase and assume the constant trajectory $\varphi_{\mathrm{cl}}=\varphi_0$ and $\varphi_{\mathrm{q}}=0$. Then we employ the charge conservation constraint, $Q_{\mathrm{L}}[\varphi_0]+Q_{\mathrm{R}}[\varphi_0]=0$, for $t_0\to\infty$ [cf. Eq. (16)] and obtain

$$\mu=\frac{\gamma_{\mathrm{L}}^2-\gamma_{\mathrm{R}}^2}{2(\gamma_{\mathrm{L}}^2+\gamma_{\mathrm{R}}^2)}V. \tag{19}$$

Unlike in the Dirac case, in which the distribution function is a two-step one governed exclusively by the voltages in the leads, in the current Majorana case there are more steps and the chemical potential is important.

III. FORMALISM AND ANALYTICAL RESULTS

A. Dissipative action

We evaluate the AES action of Eq. (15), and obtain

$$S_{\rm AES}=\iint dtdt'[u^*_{\rm cl}\quad u^*_{\rm q}]_t\begin{bmatrix}0 & \alpha^A\\ \alpha^R & i\alpha^K_{\rm M}\end{bmatrix}_{t-t'}\begin{bmatrix}u_{\rm cl}\\ u_{\rm q}\end{bmatrix}_{t'}, \tag{20}$$

where $u_{\rm cl}=e^{-\frac{i}{2}\varphi_{\rm cl}}\cos\frac{\varphi_{\rm q}}{4}$ and $u_{\rm q}=-ie^{-\frac{i}{2}\varphi_{\rm cl}}\sin\frac{\varphi_{\rm q}}{4}$ are classical and quantum parts of gauge exponents. In the quasiclassical limit, the off-diagonal terms in Eq. (20) determine the dissipative dynamics of the phase. They are given by the retarded (advanced) functions, $\alpha^{R(A)}(t)=\int\frac{d\epsilon}{2\pi}e^{-i\epsilon t}\alpha^{R(A)}_\epsilon$, with the spectra

$$\mathrm{Im}\alpha^{R(A)}_\epsilon=\pm\frac{\Gamma}{4}\sum_n\left(f_{{\rm D},E_n+\epsilon}-f_{{\rm M},E_n}\right) \tag{21}$$

(see Appendix C). The diagonal term is the Keldysh one responsible for nonequilibrium fluctuations. Its spectrum reads

$$\alpha^K_{{\rm M},\epsilon}=\frac{\Gamma}{2}\sum_n\left(1-f_{{\rm M},E_n}f_{{\rm D},E_n+\epsilon}\right). \tag{22}$$

Here, dimensionless $\Gamma=\frac{\gamma_{\rm L}^2+\gamma_{\rm R}^2}{2\pi^2v^2}$ is the coupling strength of the phase to the dissipative environment. It is the probability for a Majorana excitation to leave the island after encircling it once. In the tunneling limit, we have $\Gamma\ll1$. Also, the two-step distribution of Dirac fermions has been introduced:

$$f_{{\rm D},\epsilon}=\frac{\gamma_{\rm L}^2f_{{\rm L},\epsilon+\mu}+\gamma_{\rm R}^2f_{{\rm R},\epsilon+\mu}}{\gamma_{\rm L}^2+\gamma_{\rm R}^2}. \tag{23}$$

In the metallic limit, i.e., small level spacing, we replace the sum over n by the integral $E_{\rm Th}\sum_n\to\int dE$, and we obtain the Ohmic spectrum, $\mathrm{Im}\alpha^R_\epsilon=\frac{\Gamma}{2}\epsilon$. The Keldysh kernel reads

$$\alpha^K_{{\rm M},\epsilon}=\frac{\Gamma}{2\left(\gamma_{\rm L}^2+\gamma_{\rm R}^2\right)^2}\left[\gamma_{\rm L}^2\gamma_{\rm R}^2(|\epsilon+V|+|\epsilon-V|+2|\epsilon+2\mu|)\right.$$
$$\left.+\gamma_{\rm L}^4(|\epsilon|+|\epsilon+2\mu-V|)+\gamma_{\rm R}^4(|\epsilon|+|\epsilon+2\mu+V|)\right]. \tag{24}$$

As will be shown below, phase trajectories that contribute to the path integral have typical time scales $\sim E_{\rm c}^{-1}$. One can show that for $\epsilon\lesssim E_{\rm c}$ the kernel α^K_ϵ can be replaced by its zero-frequency value, $\alpha^K_{{\rm M},\epsilon=0}=\frac{\Gamma}{2}\xi_{\rm M}|V|$, provided

$$V\gg E_{\rm c}\max\{h,h^{-1}\}. \tag{25}$$

Here, the asymmetry parameter is defined as

$$h=\frac{\gamma_{\rm R}^2}{\gamma_{\rm L}^2}. \tag{26}$$

The parameter $\xi_{\rm M}$ is given by $\xi_{\rm M}=p_hq_h$, where

$$p_h=\frac{4h}{(1+h)^2} \tag{27}$$

and

$$q_h=1+\frac{|1-h|}{2(1+h)}. \tag{28}$$

Neglecting the frequency dependence of the kernel $\alpha^K_{{\rm M},\epsilon}$ at high voltages is similar to the common approximation for a classical noise at high temperatures. In this case, the kernel in Eq. (20) becomes local, and the AES action assumes the form $S_{\rm AES}=\int\mathcal{L}_{\rm d}[\varphi]dt$, where the effective dissipative Lagrangian $\mathcal{L}_{\rm d}[\varphi]$ reads

$$\mathcal{L}_{\rm d}[\varphi]=\frac{\Gamma}{2}\left(i\xi_{\rm M}|V|\sin^2\frac{\varphi_{\rm q}}{4}-\frac{i\dot\varphi_{\rm q}}{4}\cos\frac{\varphi_{\rm q}}{2}-\frac{\dot\varphi_{\rm cl}}{2}\sin\frac{\varphi_{\rm q}}{2}\right). \tag{29}$$

At low voltages, $V\lesssim E_{\rm c}\max\{h,h^{-1}\}$, the AES kernel becomes nonlocal in time, and our approach ceases to be accurate.

B. Formula for the current and the tunneling density of states

Due to the nonzero $E_{\rm c}$ no charge accumulation can occur on the island in the long-time limit. Therefore, at $t_0\to\infty$ we expect $\langle Q_{\rm L}\rangle=-\langle Q_{\rm R}\rangle$. Then we are allowed to consider the following symmetrized form for the current: $I=t_0^{-1}\frac{\gamma_{\rm R}^2\langle Q_{\rm L}\rangle-\gamma_{\rm L}^2\langle Q_{\rm R}\rangle}{\gamma_{\rm L}^2+\gamma_{\rm R}^2}$. Here, the average is taken over all trajectories, $\langle O\rangle=\int D[\varphi]e^{i\int(\mathcal{L}_{\rm c}[\varphi]+\mathcal{L}_{\rm d}[\varphi])dt}O[\varphi]$. After some algebra with Eq. (16), we arrive at the formula for the current,

$$I_{\rm M}=g\int\nu_{{\rm M},\omega}(n_{{\rm L},\omega}-n_{{\rm R},\omega})d\omega, \tag{30}$$

where the dimensionless conductance is $g=\frac{\gamma_{\rm L}^2\gamma_{\rm R}^2}{4\pi^2v^2(\gamma_{\rm L}^2+\gamma_{\rm R}^2)}$. As shown by Meir and Wingreen [26], the nonequilibrium state of the island is hidden in the normalized TDoS $\nu_{{\rm M},\omega}$. In the metallic limit, we obtain

$$\nu_{{\rm M},\omega}=1-\frac{1}{4\pi}\iint e^{i(\omega-\epsilon-\mu)\tau}\mathcal{D}(\tau)f_{{\rm M},\epsilon}d\epsilon d\tau. \tag{31}$$

The nontrivial contribution in Eq. (31) is provided by

$$\mathcal{D}(\tau)=P^<(\tau)-P^>(\tau), \tag{32}$$

where $P^{\lessgtr}(\tau)=\langle e^{-\frac{i}{2}\varphi(\tau_\pm)+\frac{i}{2}\varphi(0_\mp)}\rangle$ are the bosonic propagators. For brevity, the phase variables are written in the $\pm$ basis. The propagators obey the following symmetry: $P^{\lessgtr}(-\tau)=(P^{\lessgtr}(\tau))^*$.

We note that the phase propagators $P^{\gtrless}$ can be written as the averages, $P^<(\tau)=\langle b(0)b^\dagger(\tau)\rangle$ and $P^>(\tau)=\langle b^\dagger(\tau)b(0)\rangle$, with the Heisenberg bosonic operators $b=e^{\frac{i}{2}\varphi}$ and $b^\dagger=e^{-\frac{i}{2}\varphi}$. These are the ladder operators of the complex bosonic mode acting in a space of different charge states. Hence, the Fourier-transformed function $\mathcal{D}_\omega=\int\mathcal{D}(\tau)e^{i\omega\tau}d\tau$ describes the nonequilibrium excitation spectrum in the capacitor.

C. SET with the Dirac island

So far, we have considered the Majorana edge mode in the island. Here, we provide the analogous calculations for a device with a normal island that hosts a Dirac edge mode. The action $S_{\rm D}=\sum_{\sigma,\sigma'}\int_0^L dx\int\frac{d\omega}{2\pi}\bar\chi_\sigma(i\partial_t+iv\partial_x)\sigma^z_{\sigma,\sigma'}\chi_{\sigma'}$ is expressed now in terms of a complex field $\chi\neq\bar\chi$. There are following distinctions from the Majorana case. First, the nonequilibrium distribution function has the well-known double-step structure, $f_{{\rm D},\epsilon}$, which is not particle-hole symmetric, i.e., $f_{{\rm D},\epsilon}\neq-f_{{\rm D},-\epsilon}$, except the limit of fully symmetric

setup, $\gamma_L = \gamma_R$. Second, in the formula for the current,

$$I_D = g \int \nu_{D,\omega}(n_{L,\omega} - n_{R,\omega}) d\omega, \tag{33}$$

we have $\nu_{D,\omega} = 1 - \frac{1}{4\pi} \iint e^{i(\omega-\epsilon-\mu)\tau} \mathcal{D}(\tau) f_{D,\epsilon} d\epsilon d\tau$. Note that the chemical potential does not influence the result in the Dirac case. Indeed, introducing $\tilde{f}_{D,\epsilon} = f_{D,\epsilon-\mu}$, i.e., counting the energy from zero, we see that the distribution function $\tilde{f}_{D,\epsilon}$ does not depend on μ. The third distinction is that the prefactor $\xi_M = p_h q_h$ in Eq. (29) is replaced by

$$\xi_D = p_h. \tag{34}$$

It follows from the Keldysh kernel in the Dirac case, which reads

$$\alpha^K_{D,\epsilon} = \Gamma \frac{(\gamma_L^4 + \gamma_R^4)|\omega| + \gamma_L^2 \gamma_R^2 (|\omega - V| + |\omega + V|)}{(\gamma_L^2 + \gamma_R^2)^2}. \tag{35}$$

Similar to the Majorana case, the frequency dependence of this kernel can be neglected and our approach is accurate if $V \gg E_c \max\{h, h^{-1}\}$.

D. Path integration and the instanton: Boson propagator

In this section we consider the cases of Majorana and Dirac in parallel; thus, we omit the indices "M" and "D" in ξ. Calculation of boson exponents in Eq. (32) is based on the following representation of the path integral:

$$\left\langle e^{-\frac{i}{2}\varphi(\tau_\pm) + \frac{i}{2}\varphi(0_\mp)} \right\rangle = \int D[\varphi] e^{i\mathcal{S}_\pm[\varphi_q] + \int \dot{\varphi}_{cl} \mathcal{A}[\varphi_q] dt}. \tag{36}$$

Here, we have introduced

$$\mathcal{S}_\pm = \mp \frac{\varphi_q(0) + \varphi_q(\tau)}{4} + \frac{1}{2} \int \left(i\xi\Gamma |V| \sin^2 \frac{\varphi_q}{4} + \dot{\varphi}_q Q_g \right) dt, \tag{37}$$

which does not contain classical components of the phase. We have also introduced

$$\mathcal{A} = \frac{\dot{\varphi}_q(t)}{8E_c} - \frac{\Gamma}{4} \sin \frac{\varphi_q(t)}{2} + \frac{\theta(t-\tau) - \theta(t)}{2}, \tag{38}$$

which couples linearly to φ_{cl}. The linearity of the action in Eq. (36) with respect to φ_{cl} plays the central role in our solution. We remind that the exclusively linear dependence on φ_{cl} is based on two approximations: the high voltage and the Ohmic spectrum of the island. The linearity in $\dot{\varphi}_{cl}$ allows one to integrate this field out and obtain a functional δ distribution, $\int D[\varphi_{cl}] e^{i\int \dot{\varphi}_{cl} \mathcal{A}[\varphi_q] dt} = \delta(\mathcal{A}[\varphi_q])$. Therefore, the remaining path integral over φ_q is restricted by a manifold of trajectories satisfying $\mathcal{A}[\varphi_q] = 0$ with the boundary condition $\varphi_q(-\infty) = 0$. Analyzing $\mathcal{S}_\pm$ we now restrict the allowed trajectories. We note that $\mathcal{S}_\pm$ has an imaginary part $\sim i \int \sin^2 \frac{\varphi_q}{4} dt$. It provides a selection rule for the trajectories: $\exp(i\mathcal{S}_\pm) \neq 0$ only if $\varphi_q(+\infty) = 4\pi n$, $n \in \mathbb{Z}$. We find that only a single solution of the first-order differential equation $\mathcal{A}[\varphi_q] = 0$ satisfies this selection rule, $\varphi_q(t) = \Phi_\tau(t)$. Therefore, the result of the path integration for the boson propagators reads

$$P^{\gtrless}(\tau) = e^{i\mathcal{S}_\pm[\Phi_\tau(t)]}. \tag{39}$$

Note that the combination of θ functions in the right-hand side of the equation for the quantum trajectory, $\frac{\dot{\varphi}_q(t)}{8E_c} - \frac{\Gamma}{4} \sin \frac{\varphi_q(t)}{2} = -\frac{\theta(t-\tau) - \theta(t)}{2}$, plays the role of an external force. It switches on at $t = 0$ and off at $t = \tau$ (assuming $\tau > 0$). Consider first the case of zero force when the equation is uniform, $\dot{\varphi}_q = 2E_c\Gamma \sin \frac{\varphi_q}{2}$, i.e., when $t \in [-\infty; 0] \cup [\tau; \infty]$. It has a set of trivial solutions,

$$\varphi_q = 2\pi n, \tag{40}$$

and the instantonlike ones,

$$\varphi_q = \pm 4 \arctan \left(A e^{\pi \frac{\Gamma t}{\tau_c}} \right) + 4\pi n, \tag{41}$$

with $n \in \mathbb{Z}$. Here, the constant A determines the instanton center and the time scale τ_c is inversely proportional to the charging energy, $\tau_c = \frac{\pi\hbar}{E_c}$. The instanton has slow dynamics on the long RC-like time scale, $\sim \frac{\tau_c}{\pi\Gamma}$, due to $\Gamma \ll 1$.

Consider the second case when the force is switched on ($t \in [0; \tau]$) and the equation becomes $\frac{\dot{\varphi}_q(t)}{8E_c} - \frac{\Gamma}{4} \sin \frac{\varphi_q(t)}{2} = \frac{1}{2}$. We neglect the sine term due to small $\Gamma \ll 1$ prefactor and obtain a rapidly growing linear solution

$$\varphi_q = 4E_c t + B \tag{42}$$

up to small oscillations with an amplitude $\sim\Gamma$.

We have to match the linear solution (42) in the region $t \in [0; \tau]$ with the solutions in the remaining two regions, $[-\infty; 0]$ and $[\tau; \infty]$. The analysis shows that, in order to satisfy the above selection rules, the solution in the region $t < 0$ should be of the instanton form (41) and in the other region, $t > \tau$, the constant one, Eq. (40), with an even n. The matching conditions (continuity of the solution) uniquely determine free parameters A_τ and B_τ, as well as the sign of the instanton function, and the even integer $n_\tau = 2N_\tau$, where we added the subscript τ to emphasize the τ dependence. In particular, we have

$$N_\tau = \lfloor \tau/\tau_c + 1/2 \rfloor, \tag{43}$$

where the floor function $\lfloor x \rfloor$ returns the greatest integer less than or equal to x. Note that the integer-valued function N_τ is odd, $N_\tau = -N_{-\tau}$.

After some algebra, we find the final result for the quantum trajectory at $\tau > 0$:

$$\Phi_\tau(t) = \begin{cases} \phi_\tau(t), & t < 0 \\ 4\pi N_\tau + 4E_c(t-\tau), & 0 < t < \tau \\ 4\pi N_\tau, & t > \tau. \end{cases} \tag{44}$$

The view of the solution is shown in Fig. 2 for different τ/τ_c ratios. The instanton tail in Eqs. (44) reads

$$\phi_\tau(t) = 4(-1)^{m_\tau} \arctan \left[e^{\pi \frac{\Gamma t}{\tau_c}} \tan \frac{\arccos(\cos(2\pi \frac{\tau}{\tau_c}))}{2} \right], \tag{45}$$

where the discrete -valued function m_τ, which determines the overall sign of Eq. (45), is given by $m_\tau = 1 + (\lfloor \frac{\tau}{\tau_c} + \frac{1}{2} \rfloor + \lfloor \frac{\tau}{\tau_c} \rfloor)$.

Finally, one finds for the boson correlator for arbitrary τ

$$\mathcal{D}(\tau) = 2ie^{i2\pi Q_g N_\tau} |\cos(E_c\tau)|^{\frac{\xi|V|}{2E_c}} \sin \left(\frac{\pi\tau}{\tau_c} \right) e^{-\kappa_\tau}. \tag{46}$$

This is an oscillating function of τ multiplied by a decaying envelope determined by $\kappa_\tau = \frac{\Gamma}{4} \xi |V| (|\tau| - \frac{1}{2E_c} \sin(2E_c|\tau|))$.

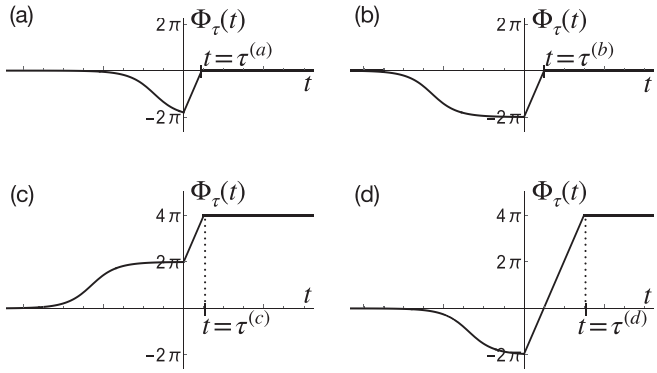

FIG. 2. Schematic view of the quantum trajectory (44). For $t<0$ it has the instanton tail $\phi_\tau(t)$ [Eq. (45)], a linear part $\sim 4E_c t$ at $0<t<\tau$, and a constant value $4\pi\mathcal{N}_\tau$ at $t>\tau$. Data shown for (a) $\tau^{(a)}=0.45\tau_c$, (b) $\tau^{(b)}=0.499\tau_c$, (c) $\tau^{(c)}=0.501\tau_c$, and (d) $\tau^{(d)}=1.49\tau_c$.

Neglecting small decay κ_τ in Eq. (46), the following spectrum of excitations is obtained:

$$\mathcal{D}_\omega=\sum_n \mathcal{W}_\omega\delta(\omega-\omega_n). \tag{47}$$

It is a ladder of levels, $\omega_n=2E_c(n-Q_g-\frac{1}{2})$, corresponding to excitations between the states with energies E_n and E_{n-1} where $E_n=E_c(n-Q_g)^2$ is the energy of a state with n excess electrons in the island. (We note that the singularities will be slightly smoothened by the frequency $\sim\Gamma E_c$ when the κ_τ is taken into account.) The envelope spectral function $\mathcal{W}_\omega$ is

$$\mathcal{W}_\omega=-8E_c\int_0^{\frac{\tau_c}{2}}|\cos E_c\tau|^{\frac{\xi|V|}{2E_c}}\sin(E_c\tau)\sin(\omega\tau)d\tau. \tag{48}$$

It is an odd function of ω, $\mathcal{W}_\omega=-\mathcal{W}_{-\omega}$. Its negative (positive) values correspond to rates of an absorption (emission) of an electron by a lead at the energy $\hbar\omega$.

In the high-voltage regime we estimate that the weights $\mathcal{W}_{\omega_n}$ are significant up to $n\sim\sqrt{\frac{V}{E_c}}$. This estimate for n determines the number of the charge states that participate in the transport.

E. Asymptotic expressions

Let us come back to the expressions for the currents, Eqs. (30) and (33), and analyze some important cases. We focus on the asymptotic behavior at voltages $V\gg E_c\max\{h,h^{-1}\}$ and integrate over ϵ and ω analytically. In this regime the decay κ_τ in Eq. (46) is negligible. The following identities for the Fourier transformations of distribution functions, $f_{M(D)}(\tau)=\int\frac{d\epsilon}{2\pi}e^{-i\epsilon\tau}f_{M(D),\epsilon}$, are used: $f_M(\tau)=-i\frac{\gamma_L^2\cos(\frac{1}{2}V\tau+\mu\tau)+\gamma_R^2\cos(\frac{1}{2}V\tau-\mu\tau)}{\pi(\gamma_L^2+\gamma_R^2)\tau}$ and $f_D(\tau)=-ie^{i\mu\tau}\frac{\gamma_L^2e^{-iV\tau/2}+\gamma_R^2e^{iV\tau/2}}{\pi(\gamma_L^2+\gamma_R^2)\tau}$. For the difference in occupation numbers in the leads, $\Delta n_\omega=n_{L,\omega}-n_{R,\omega}$, we have $\Delta n(\tau)=\int\frac{d\omega}{2\pi}e^{-i\omega\tau}\Delta n_\omega=\frac{\sin\frac{V\tau}{2}}{\pi\tau}$. Then the currents read

$$I_{M(D)}=gV-\pi g\int e^{-i\mu\tau}\mathcal{D}(\tau)f_{M(D)}(\tau)\Delta n(-\tau)d\tau. \tag{49}$$

The integrals in Eq. (49) can be split into a sum of integrals over intervals $\tau\in[\tau_c(m-\frac{1}{2});\tau_c(m+\frac{1}{2})]$, $m\in\mathbb{Z}$. Their integrands have each a narrow peak in every interval. The peak at $m=0$ is given by a smoothened singularity in $\Delta n(\tau)$. In this case, $\mathcal{D}(\tau)\approx 1$ at the relevant time scale of $\tau\sim\frac{1}{V}$. The integral for $m=0$ yields the offset current, I_{offs}. Note that it does not depend on Q_g and is proportional to E_c. Integrals over the other $m\neq 0$ peaks are responsible for the part of the current, I_{osc}, showing the gate charge oscillations. Their amplitude is much smaller than that of the offset current. This means that at high voltages the strong Coulomb blockade is weakened and the charge on the island is not well defined. For the calculation of I_{osc} the boson correlator $\mathcal{D}$ becomes important. In a $\tilde\tau$ vicinity of the mth peak, where $\tau=\tau_c m+\tilde\tau$, it reads $\mathcal{D}(\tau)=2i(-1)^m\sin(E_c\tilde\tau)e^{i2\pi Q_g m}\exp(-\frac{\xi}{4}|V|E_c\tilde\tau^2)$. Therefore, for both systems the current can be written as

$$I_{M(D)}=gV-I_{M(D),offs}-I_{M(D),osc}. \tag{50}$$

F. Offset current

The difference between Majorana and Dirac fermions is most prominent for asymmetric systems. We obtain the following asymptotic results ($V\gg E_c\max\{\frac{\gamma_R^2}{\gamma_L^2},\frac{\gamma_L^2}{\gamma_R^2}\}$) for the offset current. In the Majorana case we get

$$I_{M,offs}=g\left(1+\frac{|\gamma_R^2-\gamma_L^2|}{2(\gamma_R^2+\gamma_L^2)}\right)E_c. \tag{51}$$

In comparison, in the Dirac case we find

$$I_{D,offs}=gE_c \tag{52}$$

for an arbitrary value of γ_R^2/γ_L^2. Therefore, the deficit current in the Majorana case [cf. Eq. (51)] is up to 3/2 times larger than that in the Dirac case.

G. Gate charge oscillations

We obtain the following asymptotic result at large voltages for the Dirac case:

$$I_{D,osc}=g\,\mathrm{sgn}(V)\frac{\sinh\frac{2}{\xi_D}}{\sqrt{\pi\xi_D}}\sqrt{\frac{E_c^3}{|V|}}e^{-\frac{|V|}{\xi_D E_c}}\times\frac{F\left(\frac{V}{2E_c},Q_g\right)+hF\left(\frac{-V}{2E_c},Q_g\right)}{1+h}. \tag{53}$$

There is an exponential decay of oscillation amplitude as a function of V. The gate charge oscillation pattern is given by the function $F_{x,y}=(2\mathrm{mod}_1(-x+y+\frac{1}{2})-1)^2-\frac{1}{3}$. (The function $\mathrm{mod}_1(z)$ returns a fractional part of z.) It is found after the integration over $\tilde\tau$ in Gaussian approximation and further summation over $m\neq 0$ [30].

The function F has discontinuous derivatives. Namely, V and Q_g, which satisfy the condition $F(\frac{\pm V}{2E_c},Q_g)=1$, determine border lines of the so-called Coulomb diamond in the differential conductance map. As seen from Eq. (53), there are two sets of border lines, $Q_g^{(1,2)}=\pm\frac{V}{2E_c}+\frac{1}{2}+n$ ($n\in\mathbb{Z}$). In the asymmetric limit with $h\ll 1$ the lines $Q_g^{(2)}$ are suppressed.

In the Majorana case the result in the general case is more cumbersome:

$$I_{\mathrm{M,osc}} = \frac{g\,\mathrm{sgn}(V)}{2\sqrt{\pi\xi_{\mathrm{M}}}}\sqrt{\frac{E_{\mathrm{c}}^3}{|V|}}\left\{\frac{(h-1)\sinh\frac{4\mu}{V}}{1+h}e^{\frac{-\mu^2}{E_{\mathrm{c}}|V|\xi_{\mathrm{M}}}}F\left(\frac{\mu}{E_{\mathrm{c}}},Q_{\mathrm{g}}\right)+\sum_{j,s=\pm1}h^{\frac{1-s}{2}}\frac{\sinh\frac{2+(j+1)s\frac{2\mu}{V}}{\xi_{\mathrm{M}}}}{1+h}e^{-|V|\frac{1+2(j+1)(s+\frac{\mu}{V})\frac{\mu}{V}}{E_{\mathrm{c}}\xi_{\mathrm{M}}}}\right.$$
$$\left.\times\,F\left(\frac{jsV+(j+1)\mu}{2E_{\mathrm{c}}},Q_{\mathrm{g}}\right)\right\}. \tag{54}$$

The terms with $j=-1$ and $s=\pm1$ in the sum (54) provide the same border lines, $Q_{\mathrm{g}}^{(1,2)}=\frac{\pm V}{2E_{\mathrm{c}}}+\frac{1}{2}+n$, as in the Dirac case. Other terms define three additional sets of lines: $Q_{\mathrm{g}}^{(3,4)}=\frac{\pm V+2\mu}{2E_{\mathrm{c}}}+\frac{1}{2}+n$ and $Q_{\mathrm{g}}^{(5)}=\frac{\mu}{E_{\mathrm{c}}}+\frac{1}{2}+n$. Note that $Q_{\mathrm{g}}^{(3,4,5)}$ depend on $\mu=\frac{(1-h)V}{2(1+h)}$ and, hence, make the patterns more complicated. We also find that in two particular cases, fully symmetric ($h=1$) and absolutely asymmetric systems ($h=0$ or $h=\infty$), the patterns for I_{D} and I_{M} coincide.

H. Graphical presentation of the results

In Fig. 3 we plot the normalized differential conductance as a function of the gate charge and transport voltage for the Dirac [Figs. 3(a)–3(d)] and Majorana [Figs. 3(e)–3(h)] devices. Data are found after an exact integration over time in Eq. (49). These plots demonstrate the vanishing of the border line $Q_{\mathrm{g}}^{(2)}$ at small h in strongly asymmetric Dirac devices according to asymptotic result (53). Also, we observe the emerging of three additional border lines [Fig. 3(f)], $Q_{\mathrm{g}}^{(3,4,5)}$, in the Majorana device at $h\neq1$ predicted by Eq. (54).

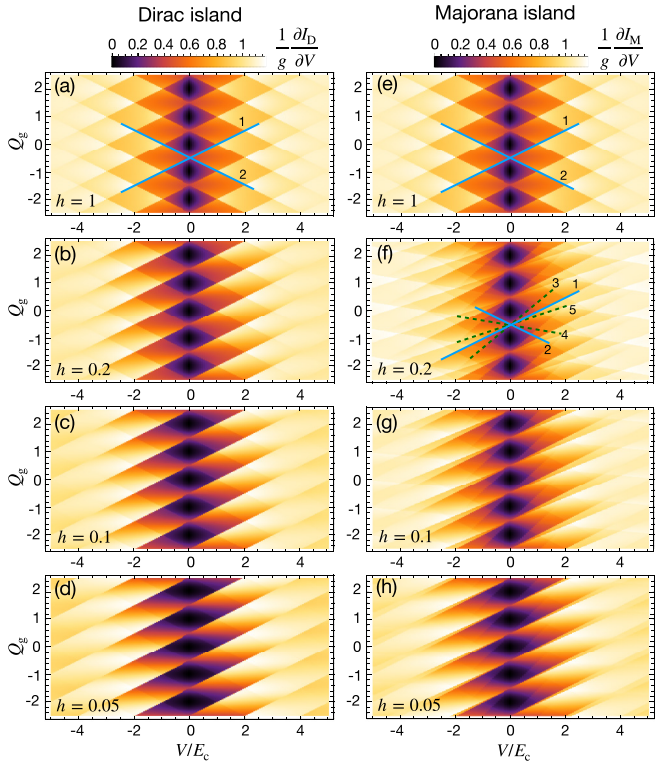

FIG. 3. Normalized differential conductances for the Dirac and Majorana SETs, $\frac{1}{g}\frac{\partial I_{\mathrm{D,M}}}{\partial V}$, plotted for different asymmetry parameters $h=\frac{\gamma_{\mathrm{R}}}{\gamma_{\mathrm{L}}}$. Left column [(a)–(d)]: $\frac{1}{g}\frac{\partial I_{\mathrm{D}}}{\partial V}$ as functions of V and Q_{g} in the Dirac case. Right column [(e)–(h)]: $\frac{1}{g}\frac{\partial I_{\mathrm{M}}}{\partial V}$ for the Majorana island. In the symmetric limit $h=1$ [(a), (e)], the patterns are identical with the border lines $Q_{\mathrm{g}}^{(1,2)}=\pm V/E_{\mathrm{c}}+\frac{1}{2}+n$ ($n\in\mathbb{Z}$). In the Dirac case with $h\neq1$ [(b)–(d)], the lines $Q_{\mathrm{g}}^{(2)}$ have smaller magnitude. In the Majorana case [(f)–(h)] the asymmetry causes three additional border lines $Q_{\mathrm{g}}^{(3,4,5)}$.

In Fig. 3 we used our formalism down to zero voltages. Quantitatively, the differential conductance at lower voltages, obtained in our formalism, is not accurate. We are confident, however, that the pattern is qualitatively correct and reflects features of the strong Coulomb blockade behavior.

In asymmetric junctions, the exponentially small oscillatory contributions are not symmetric under change of the voltage sign $V\to-V$, i.e., $I_{\mathrm{osc}}(V,Q_{\mathrm{g}})\neq-I_{\mathrm{osc}}(-V,Q_{\mathrm{g}})$. The exception is the points $Q_{\mathrm{g}}=\frac{n}{2}$ ($n\in\mathbb{Z}$) where the poles of $\mathcal{W}_\omega$ are symmetric with respect to $\omega=0$. This asymmetry is more visible at low voltages, as shown in Fig. 4 (blue solid curves). It points to a possible diodelike behavior of the asymmetric devices at low V.

In Fig. 5 we plot nonequilibrium TDoS, $\nu_{\mathrm{M},\omega}$ and $\nu_{\mathrm{D},\omega}$, which demonstrate a structure of the Coulomb gap. Note that in the Majorana case we always have a symmetric TDoS around the chemical potential μ (dashed line) for any h. It is dictated by the particle-hole symmetry of $f_{\mathrm{M},\epsilon}$. In Fig. 6 we demonstrate the broadening of the Coulomb gap when the voltage increases. Shaded regions stand for the energy domain, the states from which contribute to the electric current.

IV. DISCUSSION

The instantonlike solution presented in Eq. (44) provides only the quantum component of the phase. At the same time, the classical component is not uniquely defined and we have to integrate over all its realizations. This is precisely the difference from the nonequilibrium instanton approach developed

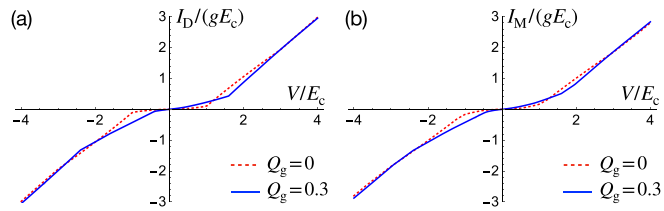

FIG. 4. Current-voltage relations $I_{\mathrm{D,M}}(V)$ for SETs with (a) Dirac and (b) Majorana islands. Solid blue curves in both panels are shown for $Q_{\mathrm{g}}=0.3$; they demonstrate the asymmetry of current-voltage relations at $Q_{\mathrm{g}}\neq n/2$ ($n\in\mathbb{Z}$). Red dashed curves correspond to the symmetric $I_{\mathrm{D,M}}(V)$ relations for $Q_{\mathrm{g}}=0$.

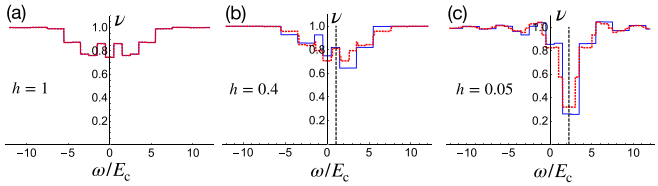

FIG. 5. Nonequilibrium TDoS in Majorana device $\nu_{M,\omega}$ (dotted red curves) and in Dirac device $\nu_{D,\omega}$ (solid blue curves). The voltage and the gate charge are chosen to be $V = 5E_c$ and $Q_g = 0$. Results are shown for (a) $h = 1$ (symmetric device, curves match), (b) $h = 0.4$, and (c) $h = 0.05$ (highly asymmetric device). In the Majorana case, the TDoS is always symmetric around the chemical potential μ (vertical black dashed lines).

in Ref. [15]. This approach is valid for $g \gg 1$, i.e., for the weak Coulomb blockade, and the instanton trajectory fixes both quantum and classical phase components. In contrast, in our case $g \ll 1$, the Coulomb blockade is strong at low voltages and is lifted at voltages higher than the charging energy.

Our approach based on the AES action allows us to reproduce quantitatively some already known results obtained within charge representation. This is the offset current, which is a characteristic feature of charging effects at high voltages. In the Dirac case we found $I_{D,offs} = gE_c$, which fully coincides with the offset current in the single tunnel junction with dimensionless conductance g [2]. Another example is the threshold voltage $V = E_c$ for $Q_g = 0$ and $\gamma_R = \gamma_L$, which is two times lower than that in the "orthodox" theory. This result can be easily obtained from Ref. [10] and is due to the nonequilibrium distribution function in the dot. The Coulomb blockade is lifted above this threshold. We also reproduce the threshold value $V = E_c$ [see Fig. 3(a)].

One of the central results is the unconventional offset current found for the Majorana island, $I_{M,offs} = q_h g E_c$, where the nonuniversal prefactor $1 \leqslant q_h \leqslant \frac{3}{2}$ [cf. Eq. (28)] depends on the asymmetry of the SET. This could serve as an evidence of the nonequilibrium chiral Majorana fermions in the island. In addition, the gate charge oscillations show distinctive features in the Majorana case, as shown in Fig. 3(f). Such measurements could provide an alternative to the interferometry [31–41] or time-resolved transport [42–47] in Majorana devices.

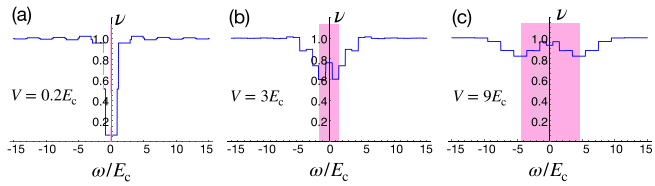

FIG. 6. Coulomb gap structure at $\gamma_R = \gamma_L$, where $\nu = \nu_M = \nu_D$, for zero offset charge and different voltages: (a) $V = 0.2E_c$, (b) $V = 3E_c$, and (c) $V = 9E_c$. The shaded areas are the energy windows $\frac{-eV}{2} < \hbar\omega < \frac{eV}{2}$ relevant for the charge transport.

V. SUMMARY

In this work, we studied the nonequilibrium transport in single-electron transistors where the strong Coulomb blockade is suppressed by large voltages. Two different kinds of quantum dots were considered. These are the islands with chiral Dirac or chiral Majorana circular modes. These could be the edge states of the usual or anomalous quantum Hall insulators (Dirac) or of the proximity-induced 2D topological superconductors (Majorana). The results of this work are twofold. First, we calculated the nonequilibrium tunneling density of states and current-voltage relations. We found an unusual behavior of the offset current in the Majorana case. There are also distinctive features in the residual gate charge oscillations of the transport current (Coulomb diamond) in the Majorana case. Second, on the methodological level, we developed an instantonlike approach in the Keldysh formalism in the limit of small conductances and high voltages.

ACKNOWLEDGMENTS

This research was financially supported by the DFG Grants No. MI 658/12-1, No. MI 658/13-1, and No. SH 81/6-1, and by RFBR Grant No. 20-52-12034.

APPENDIX A: GAUGE TRANSFORMATION

The Bogoliubov–de Gennes (BdG) Hamiltonian of the 2D topological insulator electrons ($\bar{c}_{\uparrow,\downarrow}$, $c_{\uparrow,\downarrow}$) in proximity with an s-wave superconducting island with the pairing potential $\Delta(t)$ reads

$$H(t) = \frac{1}{2}\sum_{s,s'}\int d^2\mathbf{r}[\bar{c}\ c]_s \begin{bmatrix} H_{TI}-\mathcal{V}(t) & is^y\Delta(t) \\ -is^y\Delta^*(t) & -H_{TI}^T+\mathcal{V}(t) \end{bmatrix}_{s,s'} \begin{bmatrix} c \\ \bar{c} \end{bmatrix}_{s'}. \tag{A1}$$

The Hamiltonian H_{TI} describes the topological part of the island, s is the spin index, and s^y is the Pauli matrix in the spin space. The pairing potential, $\Delta(t) = \Delta_0 e^{-2i\mu t - i\varphi(t)}$, appears after a Hubbard-Stratonovich decoupling of an interaction term in the superconducting island. The superconducting phase involves the zero mode μ, which is the yet unknown chemical potential in the superconductor. The nonzero modes are captured by $\varphi(t)$. The potential $\mathcal{V}(t)$ appears after another Hubbard-Stratonovich transformation that decouples the charging energy in the Hamiltonian. It reads as $\mathcal{V}(t) = \mathcal{V}_0 + \delta\mathcal{V}(t)$ where $\mathcal{V}_0$ is its zero mode and $\delta\mathcal{V}(t)$ involves all nonzero ones. The gauge transformation, which allows us to eliminate the phase dependence from the order parameter $\Delta(t)$ and make it real, $\Delta(t) \to \Delta_0$, reads as

$$c_s(\mathbf{r},t) \to e^{-i\mu t - i\frac{1}{2}\varphi(t)} c_s(\mathbf{r},t),\ \ \bar{c}_s(\mathbf{r},t) \to e^{i\mu t + i\frac{1}{2}\varphi(t)} \bar{c}_s(\mathbf{r},t). \tag{A2}$$

As a result, the diagonal part of the BdG Hamiltonian changes accordingly:

$$H_{TI} - \mathcal{V}(t) \to H_{TI} - (\mathcal{V}_0 - \mu) - (\delta\mathcal{V}(t) - \tfrac{1}{2}\dot{\varphi}(t)). \tag{A3}$$

The Anderson-Higgs mechanism in the superconductor suppresses the nonstationary term $(\delta\mathcal{V}(t) - \frac{1}{2}\dot{\varphi}(t))$ in Eq. (A3) [48]. Thus, we obtain the Josephson relation between the phase and potential, $\delta\mathcal{V}(t) = \frac{1}{2}\dot{\varphi}(t)$. The zero modes, $\mathcal{V}_0$ and

μ, are determined by global conditions, e.g., the capacitive relation between the charge and the potential, or the conservation of current, the latter being the main subject of our calculation. We arrive at the stationary BdG Hamiltonian (A1) with $H_{\rm TI}-(\mathcal{V}_0-\mu)$ at the diagonal, which we assume to be in the superconducting topological phase with the gap Δ_0. The low-energy excitations of Eq. (A1) are assumed to be the chiral Majorana edge modes, χ, described by the effective action (7). Assuming that transport voltages are smaller than Δ_0 and, possibly, the topological gap, the linear dispersion of the Majorana eigenstates is not affected by the presence of $(\mathcal{V}_0-\mu)$ in the BdG Hamiltonian. The gauged away phase, $\frac{1}{2}\varphi(t)+\mu t$, appears in the tunneling action (8).

APPENDIX B: CALCULATION OF THE GREEN FUNCTION OF THE CHIRAL FERMIONS IN THE ISLAND

In this Appendix we show that the local Green functions of chiral fermions at the contact points, $\mathbf{G}_{0,\epsilon}(x_{\rm L},x_{\rm L})$ and $\mathbf{G}_{0,\epsilon}(x_{\rm R},x_{\rm R})$, are equal and are denoted by $\mathbf{G}_{0,\epsilon}$ in Eq. (17). To derive $\mathbf{G}_{0,\epsilon}$ explicitly, consider the Dyson equation for the coordinate-dependent Green function of the circular chiral fermions $\mathbf{G}_0(x,t;x',t')$:

$$\mathbf{G}_0^{-1}\mathbf{G}_0(x,t;x',t')=\sigma_0\delta(x-x')\delta(t-t'). \tag{B1}$$

The stationary integral-differential operator $\mathbf{G}_0^{-1}$, which accounts for the presence of the contacts, is given by Eq. (13). After the Fourier transformation, Eq. (B1) yields

$$\Big((\epsilon+iv\partial_x)\sigma_z-\sum_{l=\rm L,R}\delta(x-x_l)\Sigma_{l,\epsilon}\Big)\mathbf{G}_\epsilon(x,x')=\sigma_0\delta(x-x'). \tag{B2}$$

We introduced here the self-energies related to the left and right tunnel contacts, $\Sigma_{l,\epsilon}=\gamma_l^2\sigma_z[\mathcal{G}_{{\rm L},\mu+\epsilon}-\mathcal{G}^T_{l,\mu-\epsilon}]\sigma_z$, where $l={\rm L},{\rm R}$. Substituting here the lead's Green functions $\mathcal{G}_l$ from Eq. (12), the self-energies read

$$\Sigma_{l,\epsilon}=-i\frac{\gamma_l^2}{2\pi v}\left((\sigma_0+\sigma_x)\frac{f_{l,\mu+\epsilon}-f_{l,\mu-\epsilon}}{2}-i\sigma_y\right). \tag{B3}$$

The next step is the Fourier transformation in a basis of eigenstates of an isolated Majorana edge mode of the length L:

$$\mathbf{G}_\epsilon(k_n,k_{n'})=L^{-2}\int_0^L dx\int_0^L dx'\mathbf{G}_\epsilon(x,x')e^{-ik_nx+ik_{n'}x'}. \tag{B4}$$

The eigenstates read e^{ik_nx} ($n\in\mathbb{Z}$) where the wave vectors and energies are given by $k_n=\epsilon_n/v$ and $\epsilon_n=E_{\rm Th}(n+n_{\rm v}/2)$, respectively. Here, $n_{\rm v}$ is an integer number, which is determined by the presence of the Berry phase and the number of vortices in the superconductor. Performing the direct and then the inverse Fourier transformations, we obtain two equations for $\mathbf{G}_\epsilon(x_{\rm L},k_{n'})$ and $\mathbf{G}_\epsilon(x_{\rm R},k_{n'})$:

$$\begin{bmatrix}\sigma_z-g_\epsilon(0)\Sigma_{{\rm L},\epsilon} & -g_\epsilon(x_{\rm L}-x_{\rm R})\Sigma_{{\rm R},\epsilon}\\ -g_\epsilon(x_{\rm R}-x_{\rm L})\Sigma_{{\rm L},\epsilon} & \sigma_0-g_\epsilon(0)\Sigma_{{\rm R},\epsilon}\end{bmatrix}\begin{bmatrix}\mathbf{G}_\epsilon(x_{\rm L},k_{n'})\\ \mathbf{G}_\epsilon(x_{\rm R},k_{n'})\end{bmatrix}=\frac{1}{L(\epsilon-\epsilon_{n'})}\begin{bmatrix}e^{ik_{n'}x_{\rm L}}\sigma_0\\ e^{ik_{n'}x_{\rm R}}\sigma_0\end{bmatrix}. \tag{B5}$$

The function $g_\epsilon(x)=\frac{1}{L}\sum_n\frac{e^{ik_nx}}{\epsilon-\epsilon_n}$ has been introduced. We need to obtain the expressions for $\mathbf{G}_\epsilon(x_{\rm L},x_{\rm L})=\sum_n\mathbf{G}_\epsilon(x_{\rm L},k_n)e^{-ik_nx_{\rm L}}$ and $\mathbf{G}_\epsilon(x_{\rm R},x_{\rm R})=\sum_n\mathbf{G}_\epsilon(x_{\rm R},k_n)e^{-ik_nx_{\rm R}}$. They follow from Eq. (B5):

$$\begin{bmatrix}\mathbf{G}_\epsilon(x_{\rm L},x_{\rm L})\\ \mathbf{G}_\epsilon(x_{\rm R},x_{\rm R})\end{bmatrix}=\sum_n\frac{1}{L(\epsilon-\epsilon_n)}\begin{bmatrix}e^{-ik_nx_{\rm L}} & 0\\ 0 & e^{-ik_nx_{\rm R}}\end{bmatrix}\begin{bmatrix}\sigma_z-g_\epsilon(0)\Sigma_{{\rm L},\epsilon} & -g_\epsilon(x_{\rm L}-x_{\rm R})\Sigma_{{\rm R},\epsilon}\\ -g_\epsilon(x_{\rm R}-x_{\rm L})\Sigma_{{\rm L},\epsilon} & \sigma_z-g_\epsilon(0)\Sigma_{{\rm R},\epsilon}\end{bmatrix}^{-1}\begin{bmatrix}e^{ik_nx_{\rm L}}\sigma_0\\ e^{ik_nx_{\rm R}}\sigma_0\end{bmatrix}. \tag{B6}$$

The obtained Green functions are given by a sequence of peaks near $\epsilon=\epsilon_n$. In the limit when the peak width, $\sim\frac{\sqrt{\gamma_{\rm L}^2+\gamma_{\rm R}^2}}{L}$, is much smaller than the level spacing, $E_{\rm Th}$, these can be replaced by δ functions. This condition of small peak broadening is equivalent to the tunnel approximation, $\gamma_{\rm L,R}\ll v$. To obtain the result in this limit, one has to drop all terms in the sum in $g_\epsilon(x)$ except those n which correspond to ϵ_n being in the vicinity of ϵ, i.e., the following replacement: $g_\epsilon(x)\to\frac{e^{ik_nx}}{L(\epsilon-\epsilon_n)}$. Reducing the result of the matrix inversion in Eq. (B6) to a Lorentzian form and approximating the Lorentzians by the δ functions, we obtain the result (17):

$$\begin{aligned}\mathbf{G}_\epsilon(x_{\rm L},x_{\rm L})=\mathbf{G}_\epsilon(x_{\rm R},x_{\rm R})&=\frac{-i}{2\pi v}\sum_n\frac{\gamma_{\rm L}^2+\gamma_{\rm R}^2}{L^2(\epsilon-\epsilon_n)^2+\frac{\left(\gamma_{\rm L}^2+\gamma_{\rm R}^2\right)^2}{4\pi^2v^2}}((\sigma_0-\sigma_x)f_{{\rm M},\epsilon}+i\sigma_y)\\ &\to-i\frac{E_{\rm Th}}{2v}\sum_n\delta(\epsilon-\epsilon_n)((\sigma_0-\sigma_x)f_{{\rm M},\epsilon}+i\sigma_y),\end{aligned} \tag{B7}$$

where the non-Fermi distribution function of the Majorana fermions reads

$$f_{{\rm M},\epsilon}=\frac{\gamma_{\rm L}^2(f_{{\rm L},\mu+\epsilon}-f_{{\rm L},\mu-\epsilon})+\gamma_{\rm R}^2(f_{{\rm R},\mu+\epsilon}-f_{{\rm R},\mu-\epsilon})}{2\left(\gamma_{\rm L}^2+\gamma_{\rm R}^2\right)}. \tag{B8}$$

APPENDIX C: DERIVATION OF THE AES ACTION

The derivation of the AES action (20) from Eq. (15) involves the following transformation under the trace:

$$\begin{aligned}\mathrm{tr}[\mathbf{G}_0\Sigma[\varphi,\eta=0]] &= \int dtdt'\mathrm{tr}_\sigma\left[\gamma_l^2\mathbf{G}_{0,t'-t}\left(U_t^+\sigma^z\mathcal{G}_{l,t-t'}\sigma^z U_{t'}-U_t\sigma^z\mathcal{G}^T_{l,t'-t}\sigma^z U_{t'}^+\right)\right]\\ &= 2\left(\gamma_\mathrm{L}^2+\gamma_\mathrm{R}^2\right)\int dtdt'\mathrm{tr}_\sigma\left[\mathbf{G}_{0,t'-t}U_t^+\sigma^z\frac{\gamma_\mathrm{L}^2\mathcal{G}_{\mathrm{L},t-t'}+\gamma_\mathrm{R}^2\mathcal{G}_{\mathrm{R},t-t'}}{\gamma_\mathrm{L}^2+\gamma_\mathrm{R}^2}\sigma^z U_{t'}\right].\end{aligned} \tag{C1}$$

We substitute here the Majorana Green function $\mathbf{G}_0$ from Eq. (17) and the lead's Green function $\mathcal{G}_l$ from Eq. (12), as well as the matrix $U_t = U[\varphi(t),\eta_l=0]$ from Eq. (9) [that depends on the field]). The symmetry of the Majorana Green function, $[\mathbf{G}_{0,-t}]^T=-\mathbf{G}_{0,t}$, has been exploited here. To obtain expression (15) we subtract the divergent stationary part $\mathrm{tr}[\mathbf{G}_0\Sigma[\varphi=\varphi_0,\eta=0]]$ from Eq. (C1). As a result, after the Keldysh rotation, we obtain the AES action (20) with $\alpha^{R(A)}$ and α^K defined by Eqs. (21) and (22). The distributions f_M and f_D, which determine the kernels α^R and α^K, originate from the dot's and leads' Green functions, $\mathbf{G}_0$ and $\mathcal{G}_{\mathrm{L,R}}$.

[1] I. O. Kulik and R. I. Shekhter, Kinetic phenomena and charge-discreteness effects in granulated media, Zh. Eksp. Teor. Fiz. **68**, 623 (1975).

[2] D. V. Averin and K. K. Likharev, Single electronics: A correlated transfer of single electrons and Cooper pairs in systems of small tunnel junctions, in *Mesoscopic Phenomena in Solids*, edited by B. L. Altshuler, P. A. Lee, and R. A. Webb (Elsevier, Amsterdam, 1991), pp. 173–271.

[3] G.-L. Ingold and Yu. V. Nazarov, Charge tunneling rates in ultrasmall junctions, *Single Charge Tunneling* (Springer, Berlin, 1992), pp. 21–107.

[4] A. Kamenev and Y. Gefen, Zero-bias anomaly in finite-size systems, Phys. Rev. B **54**, 5428 (1996).

[5] L. P. Kouwenhoven, G. Schön, and L. L. Sohn, Introduction to mesoscopic electron transport, in *Mesoscopic Electron Transport*, edited by L. L. Sohn, L. P. Kouwenhoven, and G. Schön (Springer, Dordrecht, 1997), pp. 1–44.

[6] I. L. Aleiner, P. W. Brouwer, and L. I. Glazman, Quantum effects in Coulomb blockade, Phys. Rep. **358**, 309 (2002).

[7] Y. V. Nazarov, Coulomb Blockade without Tunnel Junctions, Phys. Rev. Lett. **82**, 1245 (1999).

[8] A. Altland, L. I. Glazman, A. Kamenev, and J. S. Meyer, Inelastic electron transport in granular arrays, Ann. Phys. **321**, 2566 (2006).

[9] N. Sedlmayr, I. V. Yurkevich, and I. V. Lerner, Tunnelling density of states at Coulomb-blockade peaks, Europhys. Lett. **76**, 109 (2006).

[10] A. Altland and R. Egger, Nonequilibrium Dephasing in Coulomb Blockaded Quantum Dots, Phys. Rev. Lett. **102**, 026805 (2009).

[11] Ya. I. Rodionov, I. S. Burmistrov, and N. M. Chtchelkatchev, Relaxation dynamics of the electron distribution in the Coulomb-blockade problem, Phys. Rev. B **82**, 155317 (2010).

[12] A. Zazunov, A. L. Yeyati, and R. Egger, Coulomb blockade of Majorana-fermion-induced transport, Phys. Rev. B **84**, 165440 (2011).

[13] A. Shnirman, Y. Gefen, A. Saha, I. S. Burmistrov, M. N. Kiselev, and A. Altland, Geometric Quantum Noise of Spin, Phys. Rev. Lett. **114**, 176806 (2015).

[14] S. M. Albrecht, A. P. Higginbotham, M. Madsen, F. Kuemmeth, T. S. Jespersen, J. Nygård, P. Krogstrup, and C. M. Marcus, Exponential protection of zero modes in Majorana islands, Nature (London) **531**, 206 (2016).

[15] M. Titov and D. B. Gutman, Korshunov instantons out of equilibrium, Phys. Rev. B **93**, 155428 (2016).

[16] T. Ludwig, I. S. Burmistrov, Y. Gefen, and A. Shnirman, Strong nonequilibrium effects in spin-torque systems, Phys. Rev. B **95**, 075425 (2017).

[17] D. Pikulin, K. Flensberg, L. I. Glazman, M. Houzet, and R. M. Lutchyn, Coulomb Blockade of a Nearly Open Majorana Island, Phys. Rev. Lett. **122**, 016801 (2019).

[18] I. S. Burmistrov, Y. Gefen, D. S. Shapiro, and A. Shnirman, Mesoscopic Stoner Instability in Open Quantum Dots: Suppression of Coleman-Weinberg Mechanism by Electron Tunneling, Phys. Rev. Lett. **124**, 196801 (2020).

[19] T. Ludwig, I. S. Burmistrov, Y. Gefen, and A. Shnirman, Current noise geometrically generated by a driven magnet, Phys. Rev. Res. **2**, 023221 (2020).

[20] A. S. Dotdaev, Ya. Rodionov, and K. Tikhonov, Instantons in the out-of-equilibrium Coulomb blockade, Phys. Lett. A **419**, 127736 (2021).

[21] V. Ambegaokar, U. Eckern, and G. Schön, Quantum Dynamics of Tunneling between Superconductors, Phys. Rev. Lett. **48**, 1745 (1982).

[22] U. Eckern, G. Schön, and V. Ambegaokar, Quantum dynamics of a superconducting tunnel junction, Phys. Rev. B **30**, 6419 (1984).

[23] S. E. Korshunov, Coherent and incoherent tunneling in a Josephson junction with a "periodic" dissipation, JETP Lett. **45**, 434 (1987).

[24] L. V. Keldysh, Diagram technique for nonequilibrium processes, Zh. Eksp. Teor. Fiz. **47**, 1515 (1964) [Sov. Phys. JETP **20**, 1018 (1965)].

[25] A. Kamenev, *Field Theory of Non-Equilibrium Systems* (Cambridge University Press, Cambridge, UK, 2011).

[26] Y. Meir and N. S. Wingreen, Landauer Formula for the Current through an Interacting Electron Region, Phys. Rev. Lett. **68**, 2512 (1992).

[27] L. Fu and C. L. Kane, Superconducting Proximity Effect and Majorana Fermions at the Surface of a Topological Insulator, Phys. Rev. Lett. **100**, 096407 (2008).

[28] Q. L. He, L. Pan, A. L. Stern, E. C. Burks, X. Che, G. Yin, J. Wang, B. Lian, Q. Zhou, E. S. Choi, K. Murata, X. Kou, Z. Chen, T. Nie, Q. Shao, Y. Fan, S.-C. Zhang, K. Liu, J. Xia, and K. L. Wang, Chiral Majorana fermion modes in a quantum anomalous Hall insulator-superconductor structure, Science **357**, 294 (2017).

[29] J. Shen, J. Lyu, J. Z. Gao, Y.-M. Xie, C.-Z. Chen, C.-w. Cho, O. Atanov, Z. Chen, K. Liu, Y. J. Hu, K. Y. Yip, S. K. Goh, Q. L. He, L. Pan, K. L. Wang, K. T. Law, and R. Lortz, Spectroscopic fingerprint of chiral Majorana modes at the edge of a quantum anomalous Hall insulator/superconductor heterostructure, Proc. Natl. Acad. Sci. USA **117**, 238 (2020).

[30] The sums $\sum_n \frac{\cos An}{n^2}$ or $\sum_n \frac{\sin An}{n^2}$ are reduced to the polylogarithm function $\mathrm{Li}_2(z) = \sum_{k=1}^{\infty} \frac{z^k}{k^2}$ which has the property $\mathrm{Re}[\mathrm{Li}_2(e^{2\pi i z})] = \pi^2(\mathrm{mod}_1(z) - \frac{1}{2})^2 - \frac{\pi^2}{12}$ for real z.

[31] L. Fu and C. L. Kane, Probing Neutral Majorana Fermion Edge Modes with Charge Transport, Phys. Rev. Lett. **102**, 216403 (2009).

[32] A. R. Akhmerov, J. Nilsson, and C. W. J. Beenakker, Electrically Detected Interferometry of Majorana Fermions in a Topological Insulator, Phys. Rev. Lett. **102**, 216404 (2009).

[33] G. Strübi, W. Belzig, T. L. Schmidt, and C. Bruder, Full counting statistics of Majorana interferometers, Physica E **74**, 489 (2015).

[34] G. Strübi, W. Belzig, M.-S. Choi, and C. Bruder, Interferometric and Noise Signatures of Majorana Fermion Edge States in Transport Experiments, Phys. Rev. Lett. **107**, 136403 (2011).

[35] J. Li, G. Fleury, and M. Büttiker, Scattering theory of chiral Majorana fermion interferometry, Phys. Rev. B **85**, 125440 (2012).

[36] D. S. Shapiro, A. Shnirman, and A. D. Mirlin, Current-phase relation and h/e-periodic critical current of a chiral Josephson contact between one-dimensional Majorana modes, Phys. Rev. B **93**, 155411 (2016).

[37] D. S. Shapiro, D. E. Feldman, A. D. Mirlin, and A. Shnirman, Thermoelectric transport in junctions of Majorana and Dirac channels, Phys. Rev. B **95**, 195425 (2017).

[38] D. S. Shapiro, A. D. Mirlin, and A. Shnirman, Excess equilibrium noise in a topological SNS junction between chiral Majorana liquids, Phys. Rev. B **98**, 245405 (2018).

[39] S. B. Chung, X.-L. Qi, J. Maciejko, and S.-C. Zhang, Conductance and noise signatures of Majorana backscattering, Phys. Rev. B **83**, 100512(R) (2011).

[40] C.-X. Liu and B. Trauzettel, Helical Dirac-Majorana interferometer in a superconductor/topological insulator sandwich structure, Phys. Rev. B **83**, 220510(R) (2011).

[41] C.-Y. Hou, K. Shtengel, and G. Refael, Thermopower and Mott formula for a Majorana edge state, Phys. Rev. B **88**, 075304 (2013).

[42] B. Lian, X.-Q. Sun, A. Vaezi, X.-L. Qi, and S.-C. Zhang, Topological quantum computation based on chiral Majorana fermions, Proc. Natl. Acad. Sci. USA **115**, 10938 (2018).

[43] C. W. J. Beenakker, P. Baireuther, Y. Herasymenko, I. Adagideli, L. Wang, and A. R. Akhmerov, Deterministic Creation and Braiding of Chiral Edge Vortices, Phys. Rev. Lett. **122**, 146803 (2019).

[44] F. Hassler, A. Grabsch, M. J. Pacholski, D. O. Oriekhov, O. Ovdat, I. Adagideli, and C. W. J. Beenakker, Half-integer charge injection by a Josephson junction without excess noise, Phys. Rev. B **102**, 045431 (2020).

[45] C. W. J. Beenakker and D. O. Oriekhov, Shot noise distinguishes Majorana fermions from vortices injected in the edge mode of a chiral p-wave superconductor, SciPost Phys. **9**, 080 (2020).

[46] I. Adagideli, F. Hassler, A. Grabsch, M. Pacholski, and C. W. J. Beenakker, Time-resolved electrical detection of chiral edge vortex braiding, SciPost Phys. **8**, 013 (2020).

[47] D. S. Shapiro, A. D. Mirlin, and A. Shnirman, Microwave response of a chiral Majorana interferometer, Phys. Rev. B **104**, 035434 (2021).

[48] A. Altland and B. D. Simons, *Condensed Matter Field Theory* (Cambridge University Press, Cambridge, UK, 2010).